

SCOPE: Simulating Cross-game Operations in Playable Environments for FPS World Models

Zizhao Tong^{1,2†} Hongfeng Lai^{2†} Zeqing Wang^{2,3‡} Zhaohu Xing⁴
 Kexu Cheng¹ Haoran Xu⁵ Zhao Pu⁶ Shangwen Zhu⁶
 Ruili Feng⁷ Jian Zhao⁸ Yan Zhang³ Hao Tang⁹
 Yeying Jin^{2,3‡} Ling Shao¹

¹UCAS-Terminus AI Lab, University of Chinese Academy of Sciences ²Tencent
³National University of Singapore ⁵Zhejiang University ⁶Shanghai Jiaotong University
⁴The Hong Kong University of Science and Technology (Guangzhou) ⁷University of Waterloo
⁸Zhongguancun Institute of Artificial Intelligence
⁹State Key Laboratory of Multimedia Information Processing,
 School of Computer Science, Peking University

tongzizhao24@mails.ucas.ac.cn jinyeying@u.nus.edu ling.shao@ieee.org





 Project Page  Code  Model  Dataset



Figure 1: **SCOPE** executes complex multi-action controls and action-environment interactions (highlighted in red boxes) across diverse, unseen first-person scenes without retraining.

Abstract

Interactive world models for first-person shooter (FPS) games must resolve high-frequency overlapping control signals at every frame without disrupting unaffected

[†]This work was completed during a research internship at Tencent, supervised by Yeying Jin.

[‡]Project lead.

[✉]Corresponding Author.

regions. Existing methods inject actions globally and train on single titles, failing under dense FPS inputs. We observe that FPS actions are spatially selective: discrete events such as firing or reloading affect only a localized region around the weapon (the scope), while continuous camera and movement signals govern stable surroundings. We propose **SCOPE**, which inserts a conditioning module into each transformer block of a pretrained video diffusion model. It reshapes features into per-pixel temporal sequences so that each position computes its action response from local visual content. This separates in-scope effects from out-of-scope generation without segmentation labels. We also introduce CrossFPS, the first multi-game FPS dataset with frame-aligned action telemetry. It comprises 69K clips from 7 titles with 10-DoF controller signals, curated to remove gameplay bias. The model learns general visual-to-action mappings rather than game-specific patterns, enabling zero-shot transfer to unseen scenes. Experiments confirm strong action responsiveness, precise scope separation, and effective cross-game generalization.

1 Introduction

World models predict the consequences of actions within an environment, allowing agents to plan and interact [19, 20]. Recent video diffusion models have been interpreted as implicit world simulators [3, 60], enabling generative game engines that accept player inputs and produce visually coherent continuations [54, 15, 4]. These systems support interactive simulation across genres from Atari to Minecraft, suggesting that video generation can serve as a general substrate for world modeling.

First-person shooter (FPS) games expose a critical failure mode of this paradigm. FPS gameplay produces exceptionally dense control signals: players execute rapid camera sweeps exceeding 180°/s, interleave simultaneous firing and movement, and chain multiple discrete events within a single generation window. Current world models inject actions through global conditioning [15, 49, 10] that broadcasts a single embedding uniformly across all spatial positions. Under sparse, low-frequency controls such as open-world navigation, global injection suffices. Under the high-frequency regime of FPS, it collapses: a firing command intended for one localized region simultaneously perturbs every pixel, and rapid successive inputs compound distortions across frames. The core issue is that global conditioning cannot distinguish where in the frame each action should take effect.

We observe that FPS actions are spatially selective. Discrete events such as firing or reloading manifest only within a localized region around the weapon and immediate interaction area, which we term the scope. Everything outside the scope, including walls, sky, and distant environment, should remain stable under continuous camera and movement controls. This suggests a natural decomposition. In-scope regions require focused modeling of discrete action-to-visual correspondences, which is easier to learn in a confined spatial context than across the entire frame. Out-of-scope regions require stable scene generation driven by continuous ego-motion, which benefits from excluding in-scope dynamics so that out-of-scope synthesis is not contaminated by localized effects. Both sides demand the same primitive: per-pixel conditioning that lets each position determine whether it lies in-scope or out-of-scope from its local visual content.

Based on this observation, we propose **SCOPE**. This conditioning module is inserted into each transformer block of a pretrained video diffusion model. It reshapes features into per-pixel temporal sequences so that each position independently computes its action response from local visual content. Discrete events are processed via visually-queried cross-attention that confines effects to in-scope regions. Continuous controls are routed through temporal self-attention that models smooth ego-motion for out-of-scope generation. All modules are zero-initialized, so training begins from an unmodified video generator and progressively acquires scope separation without segmentation labels.

Existing game world models train on single titles [4, 54, 15], yet FPS games share common action-visual dynamics across titles: firing produces a muzzle flash, rightward aiming induces leftward scene flow. No prior dataset provides multi-game coverage with dense frame-aligned action annotation. We therefore introduce CrossFPS, comprising 69,000 clips across seven FPS titles with 10-dimensional controller telemetry, curated to remove gameplay bias. Training on CrossFPS enables the model to learn general visual-to-action mappings rather than game-specific patterns, allowing zero-shot transfer to unseen scenes without retraining.

Our contributions are threefold. We propose SCOPE, whose per-pixel conditioning decomposes action effects into in-scope discrete responses and out-of-scope continuous generation through end-to-end training without segmentation supervision. We introduce CrossFPS, the first multi-game FPS dataset with frame-aligned action telemetry. We demonstrate robust controllability on unseen scenes, effective zero-shot generalization, and evidence that the architecture benefits from data scaling.

2 Related Work

World Models. World models learn environment dynamics to support prediction, planning, and control [14, 19, 16, 13]. In reinforcement learning, they simulate transition dynamics before execution [48, 21, 42]. In computer vision, world models typically manifest as video generators that produce temporally coherent continuations [8, 9, 3]. A growing body of literature further pursues long-horizon consistency [63, 59, 36, 47], long-horizon memory [57], physical plausibility [56], and real-time inference [62, 70, 69]. The unifying principle is that agents rely on internal models to anticipate the outcomes of actions, whether for policy optimization in simulation or for interactive content generation. Our work falls into this category; we develop an interactive world model that conditions video generation on dense player actions, specifically maintaining structural consistency under complex, high-frequency control signals, ensuring stable frame transitions during gameplay.

Video Diffusion Models. Diffusion-based generative models [22, 46, 45] have driven rapid progress in visual synthesis. In the image domain, latent diffusion [41] and its successors [12, 40] produce high-fidelity outputs at scale. In the video domain, frameworks such as VideoCrafter [11], SVD [7], Open-Sora [68, 30], CogVideoX [61], HunyuanVideo [29], and Wan [55] achieve temporally coherent generation across diverse content. The transition to Transformer-based architectures [39, 8] has further improved generation quality and scalability, leading researchers to interpret video diffusion models as implicit physical simulators [60, 3] with applications in autonomous driving [35] and robotics [58]. Our work builds on this foundation by extending a pretrained video DiT into an interactive world model via per-pixel action conditioning, successfully mapping fine-grained input sequences to specific visual changes instead of relying on global representations.

Game World Models. Games provide natural test beds for interactive world models due to the combination of visual dynamics and rule-based logic [16]. Early GAN-based methods [27, 28] demonstrated limited generative capabilities. Subsequent diffusion-based systems [9, 38, 5, 4] have considerably advanced interactive video generation [64], enabling world models for specific titles such as Atari [4], DOOM [54], and Minecraft [15, 18]. However, existing methods are often constrained by simplified action spaces, relying on sparse discrete keystrokes [5, 54], low-dimensional continuous controls [51], or coarse text instructions [10] that fail to capture instantaneous inputs. Furthermore, injecting actions through global mechanisms, such as adaptive normalization [15, 49], cross-attention tokens [10], or latent action codes [9, 4], broadcasts a uniform action signal to all spatial positions. This conflates in-scope regions that require localized animation with out-of-scope regions that should remain stable, a mismatch that worsens under the dense, high-frequency controls of First-Person Shooter gameplay. Crucially, standard world models lack action compositionality and struggle with the simultaneous execution of hybrid controls, often causing structural artifacts or total responsiveness collapse under overlapping inputs. While certain scale-oriented models pursue cross-game generalization [38, 5, 51, 65], they require immense proprietary datasets or degrade when transferred to unseen domains with high-frequency control. In contrast, our approach, SCOPE, supports a comprehensive hybrid action space with dense, high-frequency control. By learning spatially selective action conditioning rather than expanding data volume, SCOPE achieves robust action composition and excels in zero-shot cross-game generalization across diverse environments using a compact 69K-clip dataset, establishing a highly scalable open-world simulation framework.

3 Method

3.1 Overview

Given an initial frame I_1 and a sequence of player actions $\mathbf{a}_{1:T}$ comprising continuous analog controls (camera, movement) and discrete button events (fire, reload, etc.), the model generates a video continuation $V_{2:T}$ that faithfully reflects the specified controls. This requires causal conditioning: each

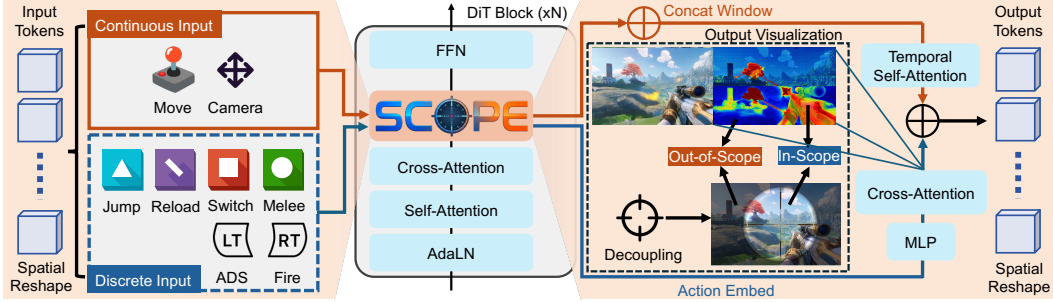


Figure 2: **SCOPE** architecture. A SCOPE module is inserted into each DiT block. Discrete inputs use cross-attention with visual queries to confine effects to in-scope regions. Continuous inputs use MLP fusion and temporal self-attention for out-of-scope generation. Pathways combine via residual connections.

frame V_t must respond to the concurrent action \mathbf{a}_t rather than merely extrapolating visual momentum. As established in Section 1, FPS actions produce spatially heterogeneous effects: discrete events should animate only in-scope regions, while continuous controls drive stable out-of-scope generation. Global action injection cannot provide this distinction.

Our method addresses this by inserting a SCOPE module into each transformer block of a pretrained video diffusion model (Figure 2). The module reshapes features into per-pixel temporal sequences and routes discrete events and continuous controls through dedicated attention pathways. Discrete events are handled via visually-queried cross-attention that confines effects to in-scope regions. Continuous controls are handled via temporal self-attention for smooth out-of-scope ego-motion. All output projections are zero-initialized so that training begins from an unmodified video generator. The entire model is trained end-to-end on CrossFPS with a flow matching objective and stochastic action dropout for Action Classifier-Free Guidance (Action-CFG) at inference.

3.2 Preliminaries

The model builds on a pretrained video Diffusion Transformer (DiT) [39] with approximately five billion parameters. A 3D VAE encoder compresses input video $\mathbf{V} \in \mathbb{R}^{3 \times T \times H \times W}$ into latent representations $\mathbf{z} \in \mathbb{R}^{C \times f \times h \times w}$, where f, h, w denote the compressed temporal, height, and width dimensions (temporal compression ratio 4, spatial compression ratio 8). The latents are patchified into a token sequence $\mathbf{x} \in \mathbb{R}^{B \times N \times D}$, where B is the batch size, $N = f \times h \times w$ is the number of tokens, and D is the hidden dimension. The backbone consists of $L = 30$ transformer blocks, each containing AdaLN, self-attention with 3D RoPE, text cross-attention, and a FFN.

We adopt flow matching [31] as the training framework. Given clean latents \mathbf{z}_0 and Gaussian noise $\epsilon \sim \mathcal{N}(0, \mathbf{I})$, noisy latents are constructed as $\mathbf{z}_t = (1 - t)\mathbf{z}_0 + t\epsilon$ for timestep $t \in [0, 1]$. The model learns to predict the velocity field $\mathbf{v}_\theta(\mathbf{z}_t, t, \mathbf{c})$ by minimizing:

$$\mathcal{L} = \mathbb{E}_{t, \mathbf{z}_0, \epsilon} \left[w(t) \|\mathbf{v}_\theta(\mathbf{z}_t, t, \mathbf{c}) - (\epsilon - \mathbf{z}_0)\|^2 \right], \quad (1)$$

where \mathbf{c} denotes conditioning signals (text, first frame) and $w(t)$ is a timestep-dependent weight. Following the image-to-video paradigm, the first-frame latent replaces the noisy latent at the first temporal position, and the loss is computed only over subsequent frames. This formulation provides a natural foundation for action-conditioned generation: we extend \mathbf{c} to include player actions via the SCOPE module described below.

3.3 SCOPE Module

The SCOPE module is inserted between text cross-attention and FFN in each of the $L = 30$ transformer blocks. It re-routes action conditioning through per-pixel temporal sequences so that each spatial location accumulates only action information relevant to its local visual content.

Action Representation. FPS gameplay produces two categories of control signals (Figure 2, left). Continuous controls $\mathbf{a}_c \in \mathbb{R}^{T_{\text{raw}} \times d_c}$ are captured from analog sticks, where T_{raw} is the number of raw gameplay frames and $d_c = 4$ covers the two movement axes and two camera axes. Discrete events $\mathbf{a}_d \in \mathbb{R}^{T_{\text{raw}} \times d_d}$ are captured from button presses, where $d_d = 6$ covers fire, ADS, reload, jump, melee, and weapon switch.

Spatial Reshape. The visual effect of any action depends on spatial content: identical inputs should produce different responses at different positions. To enable per-pixel conditioning, we reshape the token sequence \mathbf{x} into per-pixel temporal sequences:

$$\mathbf{x} \in \mathbb{R}^{B \times (f \cdot h \cdot w) \times D} \longrightarrow \hat{\mathbf{x}} \in \mathbb{R}^{(B \cdot h \cdot w) \times f \times D}, \quad (2)$$

where each of the $h \cdot w$ spatial positions now holds an independent temporal sequence of length f . All subsequent processing operates on these per-pixel sequences $\hat{\mathbf{x}}$, ensuring that in-scope and out-of-scope pixels respond differently to the same control inputs.

Dual-Pathway Processing. The two action categories are processed through dedicated pathways (Figure 2).

Discrete events trigger instantaneous, spatially localized effects: firing produces a muzzle flash, scoping triggers zoom, interactions cause localized reactions. The discrete signal \mathbf{a}_d is first embedded into action tokens via an MLP, then processed through cross-attention where the per-pixel features $\hat{\mathbf{x}}$ serve as queries and the action embeddings serve as keys and values:

$$\Delta \mathbf{x}_d = \text{CrossAttn}(Q=\hat{\mathbf{x}}, K=V=\text{MLP}_{\text{embed}}(\mathbf{a}_d)). \quad (3)$$

The output $\Delta \mathbf{x}_d$ represents per-pixel discrete action residuals. Since queries derive from local visual content, in-scope pixels attend strongly to action signals while out-of-scope pixels produce near-zero attention, confining discrete effects to relevant spatial regions. This mechanism requires no explicit region annotations; the separation emerges naturally from the visual content itself during training.

Continuous controls drive smooth ego-motion that primarily affects out-of-scope regions (scene flow from camera rotation, parallax from movement). For each latent frame i , we extract a temporal window $\mathbf{w}_i = \mathbf{a}_c[i \cdot r : i \cdot r + r \cdot s]$ of raw-frame actions, where $r = 4$ is the temporal compression ratio and s is the window size. This window is flattened and concatenated with the per-pixel feature $\hat{\mathbf{x}}$, then processed through a fusion MLP followed by temporal self-attention with RoPE:

$$\tilde{\mathbf{x}} = \text{MLP}_{\text{fuse}}([\hat{\mathbf{x}}; \text{flatten}(\mathbf{w})]), \quad \Delta \mathbf{x}_c = \text{SelfAttn}(\tilde{\mathbf{x}}, \text{RoPE}_t). \quad (4)$$

The output $\Delta \mathbf{x}_c$ represents per-pixel continuous action residuals. Because the discrete pathway already captures in-scope dynamics, the continuous pathway focuses on stable out-of-scope generation without contamination from localized effects.

The two residuals are combined and added back to the original features ($\hat{\mathbf{x}} + \Delta \mathbf{x}_c + \Delta \mathbf{x}_d$), then reshaped to the standard token layout before entering the FFN.

3.4 Training and Inference

The pretrained backbone and all $L = 30$ SCOPE modules are trained end-to-end on CrossFPS. All SCOPE output projections are zero-initialized so the model starts as an unmodified video generator and progressively learns action conditioning. This ensures training stability while enabling the backbone to co-adapt its internal representations with the action pathways. End-to-end training yields substantially stronger results than frozen or two-stage alternatives (Section 4.3). Training uses balanced sampling across all seven titles to prevent single-source dominance. The SCOPE module adds minimal parameters relative to the backbone and operates independently per spatial position, so the architecture scales naturally with larger backbones and more training data without architectural modification.

To enable tunable action intensity at inference, we apply stochastic action dropout during training: with probability p_{drop} , all action inputs ($\mathbf{a}_c, \mathbf{a}_d$) are replaced by a learnable null embedding \mathbf{a}_{null} . At inference, Action-CFG interpolates between the conditional and unconditional velocity predictions:

$$\hat{\mathbf{v}} = \mathbf{v}_\theta(\mathbf{z}_t, \mathbf{a}_{\text{null}}) + \lambda [\mathbf{v}_\theta(\mathbf{z}_t, \mathbf{a}_c, \mathbf{a}_d) - \mathbf{v}_\theta(\mathbf{z}_t, \mathbf{a}_{\text{null}})], \quad (5)$$

where the guidance scale $\lambda > 0$ controls action intensity ($\lambda=1$: standard conditioning; $\lambda>1$: amplified response; $\lambda<1$: attenuated response). Full pseudocode is provided in Appendix B.

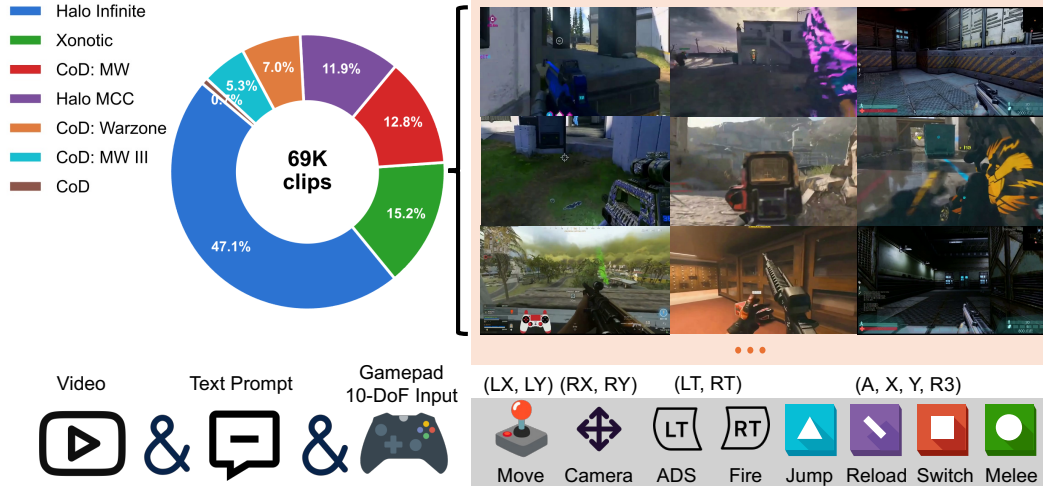


Figure 3: CrossFPS overview. Clip distribution across 7 FPS titles (69K total) with frame-aligned 10-DoF gamepad telemetry.

4 Experiments

We evaluate our method through quantitative comparison with baselines (Section 4.2), ablation studies (Section 4.3), and zero-shot generalization to unseen scenes (Section 4.4).

4.1 Setup

Pretrained model. The model builds on Wan2.2-TI2V-5B [55], a 5B-parameter video diffusion transformer with temporal compression ratio $r=4$ and spatial compression ratio 8.

Training. The backbone and 30 SCOPE modules are trained end-to-end with zero-initialized output projections. We use 480×832 resolution, 81 frames per clip (5s at 20fps), Adam with learning rate 1×10^{-5} , action dropout $p_{\text{drop}}=0.1$, and balanced game sampling. Training takes approximately 18 hours on 8 NVIDIA GPUs.

CrossFPS dataset. CrossFPS contains 69,000 five-second clips across seven FPS titles at 20fps (480×832), sourced from NitroGen [34] and WorldCam [36]. Each clip is paired with frame-aligned 10-dimensional controller telemetry (4 continuous axes + 6 discrete buttons). The dataset is split 95:3:2 into train/val/test (65,557/2,065/1,378). Three curation stages ensure cross-game consistency: Action Distribution Balancing oversamples high-intensity clips to counteract long-tail dominance; Visual-Action De-biasing retains clips with low scene-action mutual information to prevent learning game strategies; Kinetic Normalization applies optical flow-based gain calibration to align action-to-pixel-displacement ratios across titles ($\sigma_{\text{gain}}^2 = 0.034$ post-normalization). Key statistics are shown in Figure 3; full details in Appendix A.

Metrics. We measure action responsiveness via Dynamic Degree [23] and Flow Score [32]; spatial stability via Photometric Smoothness [17] and Depth Accuracy [43]; visual quality via JEPa Similarity [6, 33], FVD [53], LPIPS [67], and Motion Smoothness [17, 66]. Computation details are in Appendix C. In all tables, results are highlighted as **first**, **second**, and **third**.

Baselines. We compare against three state-of-the-art interactive world models that support action-conditioned generation: Matrix-Game 3.0 [57], LingBot-World (Act) [51], and HY-World 1.5 [49]. All three accept action signals as input but use global conditioning mechanisms. Since their native action interfaces differ from our 10-DoF telemetry format, we use Gemini [50] to translate our action sequences into the detailed natural language prompts each baseline expects.

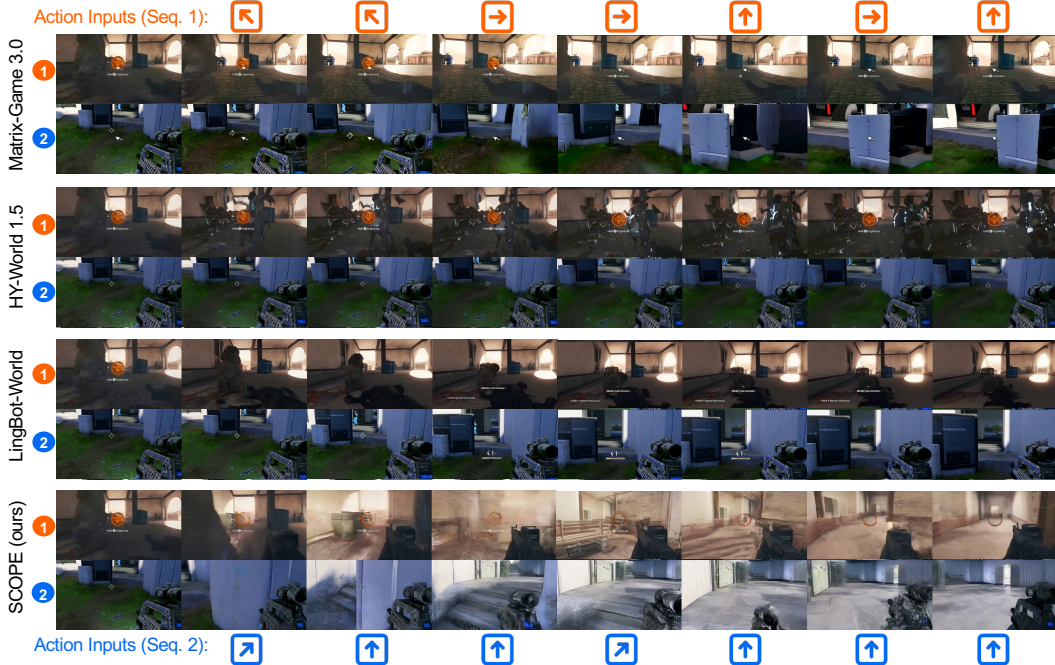


Figure 4: Qualitative comparison under high-frequency actions. Our method maintains out-of-scope stability while baselines exhibit suppressed motion, near-static output, or artifacts.

Table 1: Quantitative comparison on the CrossFPS test set.

Method	Visual Quality			Motion Quality			Consistency	
	JEPA \uparrow	FVD \downarrow	LPIPS \downarrow	Dyn.Deg. \uparrow	Flow \uparrow	Smooth \uparrow	Photo. \downarrow	Depth \downarrow
Matrix-Game 3.0	0.366	1022.7	0.692	0.661	13.36	2.502	1.194	1.524
LingBot-World (Act)	0.615	954.4	0.627	0.868	15.50	2.215	0.626	1.454
HY-World 1.5	0.464	1131.7	0.611	0.225	2.37	1.690	2.523	1.502
SCOPE	0.806	690.3	0.601	0.910	18.24	2.383	0.198	1.299

4.2 Quantitative Comparison

Table 1 shows that our method achieves the best performance on 7 of 8 metrics. The sole exception is Motion Smoothness, where Matrix-Game 3.0 leads due to action suppression rather than faithful rendering. This trade-off is expected: suppressing action responses trivially yields smoother outputs but fails the primary goal of controllability. Figure 4 confirms this qualitatively: given identical high-frequency camera rotations, our method produces smooth viewpoint changes while baselines suppress motion or introduce distortions.

The baselines receive actions through Gemini text translation rather than native telemetry, introducing an information bottleneck. To control for this modality difference, we note that the “w/o Spatial Selectivity” ablation in Table 2 uses native telemetry but replaces per-pixel conditioning with global injection, serving as a fair architectural comparison under identical input conditions. Its severe degradation (FVD 690.3 \rightarrow 885.4, Photo. 0.198 \rightarrow 0.745) confirms that the contribution is architectural rather than input-modality-driven.

Our method achieves Dynamic Degree 0.910 and Flow Score 18.24, substantially outperforming all baselines in action responsiveness. HY-World 1.5 collapses to near-static output (Dyn.Deg. 0.225) because its global normalization dilutes dense FPS signals below the effective threshold. Matrix-Game 3.0 attains moderate motion (0.661) but sacrifices responsiveness for smoothness. LingBot-World (0.868) performs best among baselines but loses discrete events unrecoverable from

Table 2: Architecture ablation on the CrossFPS test set.

Variant	Visual Quality			Motion Quality			Consistency	
	JEPA \uparrow	FVD \downarrow	LPIPS \downarrow	Dyn.Deg. \uparrow	Flow \uparrow	Smooth \uparrow	Photo. \downarrow	Depth \downarrow
SCOPE	0.806	690.3	0.601	0.910	18.24	2.383	0.198	1.299
w/o Spatial Selectivity	0.625	885.4	0.648	0.521	14.10	2.012	0.745	1.620
w/o Temporal Self-Attn	0.683	784.4	0.627	0.642	11.60	1.799	0.482	1.521
w/o Discrete Cross-Attn	0.763	725.3	0.606	0.846	17.14	2.442	0.234	1.334
w/o Action-CFG	0.740	725.8	0.610	0.820	15.90	2.405	0.280	1.350
<i>Training strategy variants</i>								
Frozen backbone	0.724	775.4	0.631	0.796	15.57	2.335	0.264	1.392
Two-stage (FT \rightarrow freeze)	0.761	732.1	0.614	0.852	17.13	2.374	0.226	1.337



Figure 5: Qualitative ablation. Left: without spatial selectivity, actions perturb the entire frame (red); with SCOPE, effects are confined (green). Right: removing pathway components causes motion degradation or in-scope element loss (red). Full model preserves both (green).

pose estimation alone. For spatial stability, Photometric Smoothness of 0.198 is $3.2\times$ better than LingBot-World (0.626) and $12.7\times$ better than HY-World (2.523), confirming scope separation without segmentation supervision. For visual quality, JEPA 0.806 (+31% over LingBot-World), FVD 690.3 (28% reduction), and LPIPS 0.601 (best) confirm that the model preserves backbone generation capability in out-of-scope regions while enabling precise in-scope responses.

4.3 Ablation Studies

All ablation variants are trained identically on the full CrossFPS dataset. Results are in Table 2.

Removing spatial selectivity causes the most severe degradation: Photometric Smoothness worsens $3.8\times$ ($0.198\rightarrow 0.745$) and Dynamic Degree drops to 0.521, reproducing global-conditioning failure modes. Removing temporal self-attention collapses Flow Score from 18.24 to 11.60, confirming that dedicated temporal modeling is essential for continuous controls. Removing discrete cross-attention causes effects to leak into out-of-scope regions (Photo. $0.198\rightarrow 0.234$) while Dynamic Degree remains high (0.846), confirming spatial confinement via visual querying. Without Action-CFG, Dynamic Degree drops to 0.820 and Flow Score to 15.90 due to regression-to-mean attenuation. Figure 5 visualizes these differences: the spatial selectivity variant produces frame-wide distortions under a fire command, whereas the full model confines effects precisely to in-scope regions.

Scalability. For training strategy (Table 2, bottom), performance improves monotonically from Frozen (FVD 775.4) through Two-stage (732.1) to End-to-end (690.3). Performance also scales with data volume and diversity without saturation, suggesting the architecture can benefit from expanded datasets (Appendix D).

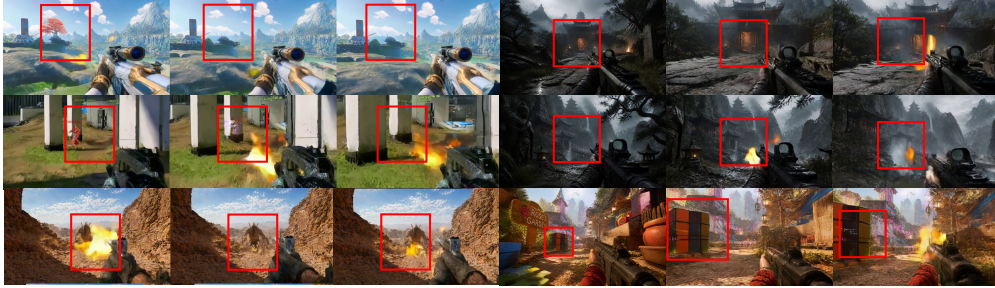


Figure 6: Action controllability on unseen scenes. Left: single and multi-action execution with in-scope effects (red boxes). Right: action-environment interactions on GPT-image-2 synthesized scenes.

Table 3: Visual quality on unseen scenes (50 clips per category, first frames from GPT-image-2).

Scene Style	JEPA \uparrow	LPIPS \downarrow	Flow \uparrow	Photo. \downarrow	Smooth \uparrow
Stylized open-world	0.772	0.618	17.45	0.235	2.341
Cooperative adventure	0.758	0.632	16.89	0.251	2.298
Mythological action	0.781	0.612	17.82	0.224	2.356
Sci-fi corridor	0.795	0.605	18.01	0.212	2.370
Average (unseen)	0.777	0.617	17.54	0.231	2.341
In-distribution (ref.)	0.806	0.601	18.24	0.198	2.383

4.4 Generalization to Unseen Scenes

To validate that the model learns general visual-to-action mappings rather than game-specific patterns, we synthesize first-person frames using GPT-image-2 [37] spanning aesthetics absent from training: stylized open-world, cooperative adventure, mythological action, and sci-fi corridor.

Visual quality. We first evaluate whether scope separation and scene stability transfer to unseen aesthetics.

Table 3 shows modest degradation relative to in-distribution performance (JEPA 0.777 vs. 0.806, Photo. 0.231 vs. 0.198). Scenes structurally similar to FPS environments (sci-fi corridors) achieve near-parity. The consistently low Photometric Smoothness across all categories (≤ 0.251) confirms that scope separation generalizes to novel visual domains.

Action controllability. We evaluate tasks at three difficulty levels: single discrete actions, multi-action compositions, and action-environment interactions. For each task, 50 videos are generated from synthesized first frames and assessed via Gemini pre-evaluation with human verification.

Table 4 shows that our method (71.5%) outperforms LingBot-World (38.3%) by 1.9 \times . The gap widens with complexity: single actions 92% vs. 78%, compositions 75% vs. 29%, environment interactions 54% vs. 21%. Matrix-Game 3.0 (0.5%) and HY-World 1.5 (8.0%) confirm that global conditioning fails on unseen scenes. Environment effects (62%) complete more reliably than object deformation (46%), reflecting the backbone’s strength in texture over geometry. Figure 6 shows qualitative examples: left columns show single and multi-action execution with in-scope effects in red boxes, right columns show NPC and environment interactions on unseen scenes.

5 Limitations and Future Work

SCOPE demonstrates effective scope separation and zero-shot transfer to unseen scenes, but its generalization currently covers cross-scene visual transfer and basic action interactions. More complex in-scope behaviors such as multi-step weapon mechanics, item usage, and fine-grained object manipulation remain challenging, due to limited interaction diversity in the training data. The model handles appearance-level responses (fire, smoke, lighting) better than geometric transformations

Table 4: Action controllability on unseen scenes. Completion rate ($N=50$ per task).

Method	Single Action		Multi-Action Composition			Action-Environment Interaction			Average
	Fire	Scope	Scope+Fire	Move+Fire	Switch+Fire	Object	Environment	NPC	
Matrix-Game 3.0	0%	0%	0%	4%	0%	0%	0%	0%	0.5%
HY-World 1.5	4%	12%	2%	36%	2%	0%	6%	2%	8.0%
LingBot-World (Act)	82%	74%	42%	18%	26%	12%	32%	20%	38.3%
SCOPE	94%	90%	82%	76%	68%	46%	62%	54%	71.5%

(structural deformation, physics-driven reactions), reflecting the texture bias of the diffusion backbone. Degraded initial frames with extreme blur also cause regression toward the average training appearance.

Despite these limitations, performance scales monotonically with data volume and diversity (Appendix D) without saturation, suggesting that richer interaction data can expand the range of learnable behaviors. In future work, we aim to extend SCOPE to long-horizon, multi-stage task execution, where the world model maintains consistent state across extended gameplay, enabling full game-level control beyond single-clip generation.

6 Conclusion

We presented SCOPE, an interactive world model for FPS games that separates in-scope and out-of-scope regions through per-pixel action conditioning. By conditioning each pixel on its local visual content rather than broadcasting global embeddings, the model learns this separation implicitly without segmentation labels. End-to-end training on CrossFPS enables co-adaptation between the pretrained backbone and the SCOPE modules, with performance scaling monotonically with data volume and diversity. From only 69K training clips, the model generalizes zero-shot to unseen game aesthetics. We believe per-pixel conditioning can extend beyond FPS to broader egocentric interactive scenarios. Extending to long-horizon stateful simulation remains an important future direction.

Acknowledgments and Disclosure of Funding

We would like to express our sincere gratitude to Ruidong Wang and Murphy Zhao for their tremendous support throughout this project. We are also deeply thankful to Shusen Wang for his invaluable assistance with technical maintenance.

References

- [1] 343 Industries. Halo: The master chief collection. <https://www.xbox.com/en-US/games/halo>, 2014.
- [2] 343 Industries. Halo infinite. <https://www.xbox.com/en-US/games/halo-infinite>, 2021.
- [3] Niket Agarwal, Arslan Ali, Maciej Bala, Yogesh Balaji, Erik Barker, Tiffany Cai, Prithvijit Chattopadhyay, Yongxin Chen, Yin Cui, Yifan Ding, et al. Cosmos world foundation model platform for physical ai. *arXiv preprint arXiv:2501.03575*, 2025.
- [4] Eloi Alonso, Adam Jelley, Vincent Micheli, Anssi Kanervisto, Amos Storkey, Tim Pearce, and François Fleuret. Diffusion for world modeling: Visual details matter in atari. *Advances in Neural Information Processing Systems*, 37:58757–58791, 2024.
- [5] Philip J. Ball, Jakob Bauer, Frank Belletti, Bethanie Brownfield, Ariel Ephrat, Shlomi Fruchter, Agrim Gupta, Kristian Holsheimer, Aleksander Holynski, Jiri Hron, Christos Kaplanis, Marjorie Limont, Matt McGill, Yanko Oliveira, Jack Parker-Holder, Frank Perbet, Guy Scully, Jeremy Shar, Stephen Spencer, Omer Tov, Ruben Villegas, Emma Wang, Jessica Yung, Cip Baetu, Jordi Berbel, David Bridson, Jake Bruce, Gavin Buttimore, Sarah Chakera, Bilva Chandra, Paul Collins, Alex Cullum, Bogdan Damoc, Vibha Dasagi, Maxime Gazeau, Charles Gbadamosi, Woohyun Han, Ed Hirst, Ashyana Kachra, Lucie Kerley, Kristian Kjems, Eva Knoepfel, Vika Koriakin, Jessica Lo, Cong Lu, Zeb Mehring, Alex Moufarek, Henna Nandwani, Valeria Oliveira, Fabio Pardo, Jane Park, Andrew Pierson, Ben Poole, Helen Ran, Tim Salimans, Manuel Sanchez, Igor Saprykin, Amy Shen, Sailesh Sidhwani, Duncan Smith, Joe Stanton, Hamish Tomlinson, Dimple Vijaykumar, Luyu Wang, Piers Wingfield, Nat Wong, Keyang Xu, Christopher

- Yew, Nick Young, Vadim Zubov, Douglas Eck, Dumitru Erhan, Koray Kavukcuoglu, Demis Hassabis, Zoubin Ghahramani, Raia Hadsell, Aäron van den Oord, Inbar Mosseri, Adrian Bolton, Satinder Singh, and Tim Rocktäschel. Genie 3: A new frontier for world models, 2025.
- [6] Adrien Bardes, Quentin Garrido, Jean Ponce, Xinlei Chen, Michael Rabbat, Yann LeCun, Mido Assran, and Nicolas Ballas. V-jepa: latent video prediction for visual representation learning (2024). In *URL* <https://openreview.net/forum>, 2024.
- [7] Andreas Blattmann, Tim Dockhorn, Sumith Kulal, Daniel Mendelevitch, Maciej Kilian, Dominik Lorenz, Yam Levi, Zion English, Vikram Voleti, Adam Letts, et al. Stable video diffusion: Scaling latent video diffusion models to large datasets. *arXiv preprint arXiv:2311.15127*, 2023.
- [8] Tim Brooks, Bill Peebles, Connor Holmes, Will DePue, Yufei Guo, Leo Jing, David Schnurr, Joe Taylor, Troy Luhman, Eric Luhman, et al. Video generation models as world simulators. *OpenAI Blog*, 1(8):1, 2024.
- [9] Jake Bruce, Michael D Dennis, Ashley Edwards, Jack Parker-Holder, Yuge Shi, Edward Hughes, Matthew Lai, Aditi Mavalankar, Richie Steigerwald, Chris Apps, et al. Genie: Generative interactive environments. In *Forty-first International Conference on Machine Learning*, 2024.
- [10] Haoxuan Che, Xuanhua He, Quande Liu, Cheng Jin, and Hao Chen. Gamegen-x: Interactive open-world game video generation. *arXiv preprint arXiv:2411.00769*, 2024.
- [11] Haoxin Chen, Yong Zhang, Xiaodong Cun, Menghan Xia, Xintao Wang, Chao Weng, and Ying Shan. Videocrafter2: Overcoming data limitations for high-quality video diffusion models. In *Proceedings of the IEEE/CVF conference on computer vision and pattern recognition*, pages 7310–7320, 2024.
- [12] Junsong Chen, Jincheng Yu, Chongjian Ge, Lewei Yao, Enze Xie, Yue Wu, Zhongdao Wang, James Kwok, Ping Luo, Huchuan Lu, et al. Pixart- α : Fast training of diffusion transformer for photorealistic text-to-image synthesis. *arXiv preprint arXiv:2310.00426*, 2023.
- [13] Meng Chu, Xuan Billy Zhang, Kevin Qinghong Lin, Lingdong Kong, Jize Zhang, Teng Tu, Weijian Ma, Ziqi Huang, Senqiao Yang, Wei Huang, et al. Agentic world modeling: Foundations, capabilities, laws, and beyond. *arXiv preprint arXiv:2604.22748*, 2026.
- [14] Kenneth James Williams Craik. *The nature of explanation*, volume 445. CUP Archive, 1967.
- [15] Etched Decart, Quinn McIntyre, Spruce Campbell, Xinlei Chen, and Robert Wachen. Oasis: A universe in a transformer. *URL: <https://oasis-model.github.io>*, 2(3):6, 2024.
- [16] Jingtao Ding, Yunke Zhang, Yu Shang, Yuheng Zhang, Zefang Zong, Jie Feng, Yuan Yuan, Hongyuan Su, Nian Li, Nicholas Sukiennik, et al. Understanding world or predicting future? a comprehensive survey of world models. *ACM Computing Surveys*, 58(3):1–38, 2025.
- [17] Haoyi Duan, Hong-Xing Yu, Sirui Chen, Li Fei-Fei, and Jiajun Wu. Worldscore: A unified evaluation benchmark for world generation. In *Proceedings of the IEEE/CVF International Conference on Computer Vision*, pages 27713–27724, 2025.
- [18] Junliang Guo, Yang Ye, Tianyu He, Haoyu Wu, Yushu Jiang, Tim Pearce, and Jiang Bian. Mineworld: a real-time and open-source interactive world model on minecraft. *arXiv preprint arXiv:2504.08388*, 2025.
- [19] David Ha and Jürgen Schmidhuber. World models. *arXiv preprint arXiv:1803.10122*, 2(3):440, 2018.
- [20] Danijar Hafner, Timothy Lillicrap, Jimmy Ba, and Mohammad Norouzi. Dream to control: Learning behaviors by latent imagination, 2019.
- [21] Danijar Hafner, Jurgis Pasukonis, Jimmy Ba, and Timothy Lillicrap. Mastering diverse control tasks through world models. *Nature*, 640(8059):647–653, 2025.
- [22] Jonathan Ho, Ajay Jain, and Pieter Abbeel. Denoising diffusion probabilistic models. *Advances in neural information processing systems*, 33:6840–6851, 2020.
- [23] Ziqi Huang, Yanan He, Jiashuo Yu, Fan Zhang, Chenyang Si, Yuming Jiang, Yuanhan Zhang, Tianxing Wu, Qingyang Jin, Nattapol Chanpaisit, et al. Vbench: Comprehensive benchmark suite for video generative models. In *Proceedings of the IEEE/CVF Conference on Computer Vision and Pattern Recognition*, pages 21807–21818, 2024.
- [24] Infinity Ward. Call of duty. <https://www.callofduty.com>, 2003.

- [25] Infinity Ward. Call of duty: Modern warfare. <https://www.callofduty.com/modernwarfare>, 2019.
- [26] Infinity Ward and Raven Software. Call of duty: Warzone. <https://www.callofduty.com/warzone>, 2020.
- [27] Seung Wook Kim, Jonah Philion, Antonio Torralba, and Sanja Fidler. Drivegan: Towards a controllable high-quality neural simulation. In *Proceedings of the IEEE/CVF Conference on Computer Vision and Pattern Recognition*, pages 5820–5829, 2021.
- [28] Seung Wook Kim, Yuhao Zhou, Jonah Philion, Antonio Torralba, and Sanja Fidler. Learning to simulate dynamic environments with gamegan. In *Proceedings of the IEEE/CVF conference on computer vision and pattern recognition*, pages 1231–1240, 2020.
- [29] Weijie Kong, Qi Tian, Zijian Zhang, Rox Min, Zuozhuo Dai, Jin Zhou, Jiangfeng Xiong, Xin Li, Bo Wu, Jianwei Zhang, et al. Hunyuanvideo: A systematic framework for large video generative models. *arXiv preprint arXiv:2412.03603*, 2024.
- [30] Bin Lin, Yunyang Ge, Xinhua Cheng, Zongjian Li, Bin Zhu, Shaodong Wang, Xianyi He, Yang Ye, Shenghai Yuan, Liuhan Chen, et al. Open-sora plan: Open-source large video generation model. *arXiv preprint arXiv:2412.00131*, 2024.
- [31] Yaron Lipman, Ricky TQ Chen, Heli Ben-Hamu, Maximilian Nickel, and Matt Le. Flow matching for generative modeling. *arXiv preprint arXiv:2210.02747*, 2022.
- [32] Yaofang Liu, Xiaodong Cun, Xuebo Liu, Xintao Wang, Yong Zhang, Haoxin Chen, Yang Liu, Tiejiong Zeng, Raymond Chan, and Ying Shan. Evalcrafter: Benchmarking and evaluating large video generation models. In *Proceedings of the IEEE/CVF conference on computer vision and pattern recognition*, pages 22139–22149, 2024.
- [33] Ge Ya Luo, Gian Mario Favero, Zhi Hao Luo, Alexia Jolicoeur-Martineau, and Christopher Pal. Beyond fvd: Enhanced evaluation metrics for video generation quality. *arXiv preprint arXiv:2410.05203*, 2024.
- [34] Loïc Magne, Anas Awadalla, Guanzhi Wang, Yinzen Xu, Joshua Belofsky, Fengyuan Hu, Jooheon Kim, Ludwig Schmidt, Georgia Gkioxari, Jan Kautz, et al. Nitrogen: An open foundation model for generalist gaming agents. *arXiv preprint arXiv:2601.02427*, 2026.
- [35] Chen Min, Dawei Zhao, Liang Xiao, Jian Zhao, Xinli Xu, Zheng Zhu, Lei Jin, Jianshu Li, Yulan Guo, Junliang Xing, et al. Driveworld: 4d pre-trained scene understanding via world models for autonomous driving. In *Proceedings of the IEEE/CVF conference on computer vision and pattern recognition*, pages 15522–15533, 2024.
- [36] Jisu Nam, Yicong Hong, Chun-Hao Paul Huang, Feng Liu, JoungBin Lee, Jiyoung Kim, Siyoon Jin, Yunsung Lee, Jaeyoon Jung, Suhwan Choi, et al. Worldcam: Interactive autoregressive 3d gaming worlds with camera pose as a unifying geometric representation. *arXiv preprint arXiv:2603.16871*, 2026.
- [37] OpenAI. Introducing ChatGPT images 2.0. <https://openai.com/index/introducing-chatgpt-images-2-0/>, 2026.
- [38] Jack Parker-Holder, Philip Ball, Jake Bruce, Vibhavari Dasagi, Kristian Holsheimer, Christos Kaplanis, Alexandre Moufarek, Guy Scully, Jeremy Shar, Jimmy Shi, et al. Genie 2: A large-scale foundation world model. URL: <https://deepmind.google/discover/blog/genie-2-a-large-scale-foundation-world-model>, 2, 2024.
- [39] William Peebles and Saining Xie. Scalable diffusion models with transformers. In *Proceedings of the IEEE/CVF international conference on computer vision*, pages 4195–4205, 2023.
- [40] Dustin Podell, Zion English, Kyle Lacey, Andreas Blattmann, Tim Dockhorn, Jonas Müller, Joe Penna, and Robin Rombach. Sdxl: Improving latent diffusion models for high-resolution image synthesis, 2023.
- [41] Robin Rombach, Andreas Blattmann, Dominik Lorenz, Patrick Esser, and Björn Ommer. High-resolution image synthesis with latent diffusion models. In *Proceedings of the IEEE/CVF conference on computer vision and pattern recognition*, pages 10684–10695, 2022.
- [42] Julian Schrittwieser, Ioannis Antonoglou, Thomas Hubert, Karen Simonyan, Laurent Sifre, Simon Schmitt, Arthur Guez, Edward Lockhart, Demis Hassabis, Thore Graepel, et al. Mastering atari, go, chess and shogi by planning with a learned model. *Nature*, 588(7839):604–609, 2020.
- [43] Yu Shang, Zhuohang Li, Yiding Ma, Weikang Su, Xin Jin, Ziyong Wang, Lei Jin, Xin Zhang, Yinzhou Tang, Haisheng Su, et al. Worldarena: A unified benchmark for evaluating perception and functional utility of embodied world models. *arXiv preprint arXiv:2602.08971*, 2026.

- [44] Sledgehammer Games. Call of duty: Modern warfare iii. <https://www.callofduty.com/store/games/modernwarfare3>, 2023.
- [45] Yang Song and Stefano Ermon. Generative modeling by estimating gradients of the data distribution, 2019.
- [46] Yang Song, Jascha Sohl-Dickstein, Diederik P Kingma, Abhishek Kumar, Stefano Ermon, and Ben Poole. Score-based generative modeling through stochastic differential equations, 2020.
- [47] Wenqiang Sun, Haiyu Zhang, Haoyuan Wang, Junta Wu, Zehan Wang, Zhenwei Wang, Yunhong Wang, Jun Zhang, Tengfei Wang, and Chunchao Guo. Worldplay: Towards long-term geometric consistency for real-time interactive world modeling. *arXiv preprint arXiv:2512.14614*, 2025.
- [48] Richard S Sutton. Dyna, an integrated architecture for learning, planning, and reacting. *ACM Sigart Bulletin*, 2(4):160–163, 1991.
- [49] Junshu Tang, Jiacheng Liu, Jiaqi Li, Longhuang Wu, Haoyu Yang, Penghao Zhao, Siruis Gong, Xiang Yuan, Shuai Shao, Linfeng Zhang, et al. Hunyuan-gamescraft-2: Instruction-following interactive game world model. *arXiv preprint arXiv:2511.23429*, 2025.
- [50] Gemini Team, Rohan Anil, Sebastian Borgeaud, Jean-Baptiste Alayrac, Jiahui Yu, Radu Soricut, Johan Schalkwyk, Andrew M Dai, Anja Hauth, Katie Millican, et al. Gemini: a family of highly capable multimodal models. *arXiv preprint arXiv:2312.11805*, 2023.
- [51] Robbyant Team, Zelin Gao, Qiuyu Wang, Yanhong Zeng, Jiapeng Zhu, Ka Leong Cheng, Yixuan Li, Hanlin Wang, Yinghao Xu, Shuailei Ma, et al. Advancing open-source world models. *arXiv preprint arXiv:2601.20540*, 2026.
- [52] Team Xonotic. Xonotic. <https://xonotic.org/>, 2011.
- [53] Thomas Unterthiner, Sjoerd Van Steenkiste, Karol Kurach, Raphael Marinier, Marcin Michalski, and Sylvain Gelly. Towards accurate generative models of video: A new metric & challenges. *arXiv preprint arXiv:1812.01717*, 2018.
- [54] Dani Valevski, Yaniv Leviathan, Moab Arar, and Shlomi Fruchter. Diffusion models are real-time game engines. *arXiv preprint arXiv:2408.14837*, 2024.
- [55] Team Wan, Ang Wang, Baole Ai, Bin Wen, Chaojie Mao, Chen-Wei Xie, Di Chen, Feiwu Yu, Haiming Zhao, Jianxiao Yang, et al. Wan: Open and advanced large-scale video generative models. *arXiv preprint arXiv:2503.20314*, 2025.
- [56] Jing Wang, Ao Ma, Ke Cao, Jun Zheng, Zhanjie Zhang, Jiasong Feng, Shanyuan Liu, Yuhang Ma, Bo Cheng, Dawei Leng, et al. Wisa: World simulator assistant for physics-aware text-to-video generation. *arXiv preprint arXiv:2503.08153*, 2025.
- [57] Zile Wang, Zexiang Liu, Jaixing Li, Kaichen Huang, Baixin Xu, Fei Kang, Mengyin An, Peiyu Wang, Biao Jiang, Yichen Wei, et al. Matrix-game 3.0: Real-time and streaming interactive world model with long-horizon memory. *arXiv preprint arXiv:2604.08995*, 2026.
- [58] Philipp Wu, Alejandro Escontrela, Danijar Hafner, Pieter Abbeel, and Ken Goldberg. Daydreamer: World models for physical robot learning. In *Conference on robot learning*, pages 2226–2240. PMLR, 2023.
- [59] Zeqi Xiao, Yushi Lan, Yifan Zhou, Wenqi Ouyang, Shuai Yang, Yanhong Zeng, and Xingang Pan. Worldmem: Long-term consistent world simulation with memory, 2025.
- [60] Sherry Yang, Yilun Du, Kamyar Ghasemipour, Jonathan Tompson, Leslie Kaelbling, Dale Schuurmans, and Pieter Abbeel. Learning interactive real-world simulators. *arXiv preprint arXiv:2310.06114*, 2023.
- [61] Zhuoyi Yang, Jiayan Teng, Wendi Zheng, Ming Ding, Shiyu Huang, Jiazheng Xu, Yuanming Yang, Wenyi Hong, Xiaohan Zhang, Guanyu Feng, et al. Cogvideox: Text-to-video diffusion models with an expert transformer. *arXiv preprint arXiv:2408.06072*, 2024.
- [62] Tianwei Yin, Michaël Gharbi, Richard Zhang, Eli Shechtman, Fredo Durand, William T Freeman, and Taesung Park. One-step diffusion with distribution matching distillation. In *Proceedings of the IEEE/CVF conference on computer vision and pattern recognition*, pages 6613–6623, 2024.
- [63] Jiwen Yu, Jianhong Bai, Yiran Qin, Quande Liu, Xintao Wang, Pengfei Wan, Di Zhang, and Xihui Liu. Context as memory: Scene-consistent interactive long video generation with memory retrieval. In *Proceedings of the SIGGRAPH Asia 2025 Conference Papers*, pages 1–11, 2025.

- [64] Jiwen Yu, Yiran Qin, Haoxuan Che, Quande Liu, Xintao Wang, Pengfei Wan, Di Zhang, Kun Gai, Hao Chen, and Xihui Liu. A survey of interactive generative video. *arXiv preprint arXiv:2504.21853*, 2025.
- [65] Jiwen Yu, Yiran Qin, Xintao Wang, Pengfei Wan, Di Zhang, and Xihui Liu. Gamefactory: Creating new games with generative interactive videos. In *Proceedings of the IEEE/CVF International Conference on Computer Vision*, pages 11590–11599, 2025.
- [66] Guozhen Zhang, Chunxu Liu, Yutao Cui, Xiaotong Zhao, Kai Ma, and Limin Wang. Vfimamba: Video frame interpolation with state space models. *Advances in Neural Information Processing Systems*, 37:107225–107248, 2024.
- [67] Richard Zhang, Phillip Isola, Alexei A Efros, Eli Shechtman, and Oliver Wang. The unreasonable effectiveness of deep features as a perceptual metric. In *Proceedings of the IEEE conference on computer vision and pattern recognition*, pages 586–595, 2018.
- [68] Zangwei Zheng, Xiangyu Peng, Tianji Yang, Chenhui Shen, Shenggui Li, Hongxin Liu, Yukun Zhou, Tianyi Li, and Yang You. Open-sora: Democratizing efficient video production for all. *arXiv preprint arXiv:2412.20404*, 2024.
- [69] Haoyi Zhu, Haozhe Liu, Yuyang Zhao, Tian Ye, Junsong Chen, Jincheng Yu, Tong He, Song Han, and Enze Xie. Sana-wm: Efficient minute-scale world modeling with hybrid linear diffusion transformer. *arXiv preprint arXiv:2605.15178*, 2026.
- [70] Hongzhou Zhu, Min Zhao, Guande He, Hang Su, Chongxuan Li, and Jun Zhu. Causal forcing: Autoregressive diffusion distillation done right for high-quality real-time interactive video generation. *arXiv preprint arXiv:2602.02214*, 2026.

A CrossFPS Dataset Details

This appendix provides complete details on the CrossFPS dataset, organized as follows: Section A.1 presents the dataset overview and per-game statistics; Section A.2 specifies the action telemetry format; Section A.3 describes the data processing pipeline; and Section A.4 details the text caption generation procedure.

A.1 Overview and Statistics

CrossFPS comprises 69,000 five-second clips across seven FPS titles at 20 fps (480×832), sourced from two public repositories: NitroGen [34], which provides gameplay recordings with frame-aligned controller telemetry for the Halo and Call of Duty series, and WorldCam [36], which contributes Xonotic recordings. The dataset is split 95:3:2 into train/val/test sets. Per-game statistics are reported in Table 5.

Table 5: **CrossFPS per-game statistics.** All clips are 5 seconds at 20 fps with 480×832 resolution.

Game	Total	Train	Val	Test
Halo Infinite [2]	32,466	30,844	973	649
Xonotic [52]	10,460	9,938	313	209
Call of Duty: Modern Warfare [25]	8,853	8,411	265	177
Halo [1]	8,227	7,817	246	164
Call of Duty: Warzone [26]	4,818	4,578	144	96
Call of Duty: Modern Warfare III [44]	3,662	3,480	109	73
Call of Duty [24]	514	489	15	10
Total	69,000	65,557	2,065	1,378

Beyond per-game volume, Table 6 summarizes the kinematic properties and diversity of CrossFPS after processing. All statistics are computed across the 65,557 training clips with continuous signals normalized to $[-1, 1]$. The corresponding distributions are visualized in Figure 7.

The high mean linear velocity (0.48) results from the $\geq 70\%$ activity filter. The angular velocity (0.26 ± 0.18) covers both precision aiming and rapid flicks, corresponding to approximately 30° – $60^\circ/s$ at 20 fps. The peak angular acceleration (0.78 ± 0.14) confirms abundant high-frequency events (flick shots, 180-degree snap turns) that stress-test scene stability (Figure 7a–c).

Table 6: CrossFPS dataset statistics after processing. Continuous signals normalized to $[-1, 1]$.

Metric	Value (Mean \pm SD)
<i>Action Intensity</i>	
Linear Velocity (v_{lin})	0.48 ± 0.12
Angular Velocity (ω_{ang})	0.26 ± 0.18
Peak Angular Accel. (α_{peak})	0.78 ± 0.14
Control Smoothness	0.82 ± 0.09
<i>Distribution</i>	
Action Entropy (H)	2.94 ± 0.31 bits
Gaze Center-bias Index	0.42 ± 0.08
Strafe-to-Forward Ratio	0.38 : 1.0
Discrete Event Density	$14.2\% \pm 3.5\%$
<i>Cross-Game Consistency</i>	
Optical Flow-Action Corr. (r)	0.91 ± 0.03
Inter-game Gain Variance	0.034

The action entropy of 2.94 ± 0.31 bits approaches the theoretical maximum for the discretized 10-dimensional action space, substantially exceeding typical human gameplay entropy. This confirms training without human bias: the model cannot rely on simple temporal priors and must learn physical action-visual mappings. Figure 7d shows the entropy shift after de-biasing ($1.85 \rightarrow 2.94$ bits). The strafe-to-forward ratio of 0.38 : 1.0 is significantly higher than navigation datasets (typically < 0.1), introducing motion parallax that forces correct in-scope/out-of-scope separation (Figure 7e). The gaze center-bias index (0.42 ± 0.08) is lower than typical human play (0.65) and professional players (0.72), confirming diverse view angles from de-biasing.

The post-normalization gain variance of 0.034 validates kinetic normalization. Before calibration, the variance across engines exceeds 0.8 (identical stick displacement produces 10° rotation in Halo but 30° in Call of Duty), causing gradient conflicts during joint training. After normalization, all titles share a unified action space with $r = 0.91 \pm 0.03$ between input and optical flow (Figure 7f).

A.2 Action Telemetry Format

Each clip is paired with per-frame 10-dimensional controller telemetry organized into four functional groups (Table 7): Movement (4 continuous axes from the left analog stick), Camera (2 continuous axes from the right analog stick), Combat (3 discrete buttons), and Utility (3 discrete buttons). The continuous signals capture analog intensity (e.g., partial stick deflection for slow movement), while discrete signals are binary indicators sampled at each frame.

Table 7: **Action telemetry format.** 10 dimensions organized into 4 functional groups.

Group	Input	Type	Description
MOVEMENT	LX	continuous	Move left / right
	LY	continuous	Move forward / back
CAMERA	RX	continuous	Turn left / right
	RY	continuous	Look up / down
COMBAT	RT	discrete	Fire
	LT	discrete	Aim down sights (ADS)
	R3	discrete	Melee
UTILITY	A	discrete	Jump
	X	discrete	Reload
	Y	discrete	Switch weapon

A.3 Data Processing Pipeline

A key design goal of CrossFPS is to eliminate human bias—the tendency of skilled players to execute stereotyped action patterns (e.g., always firing at highlighted enemies or crouching behind cover).

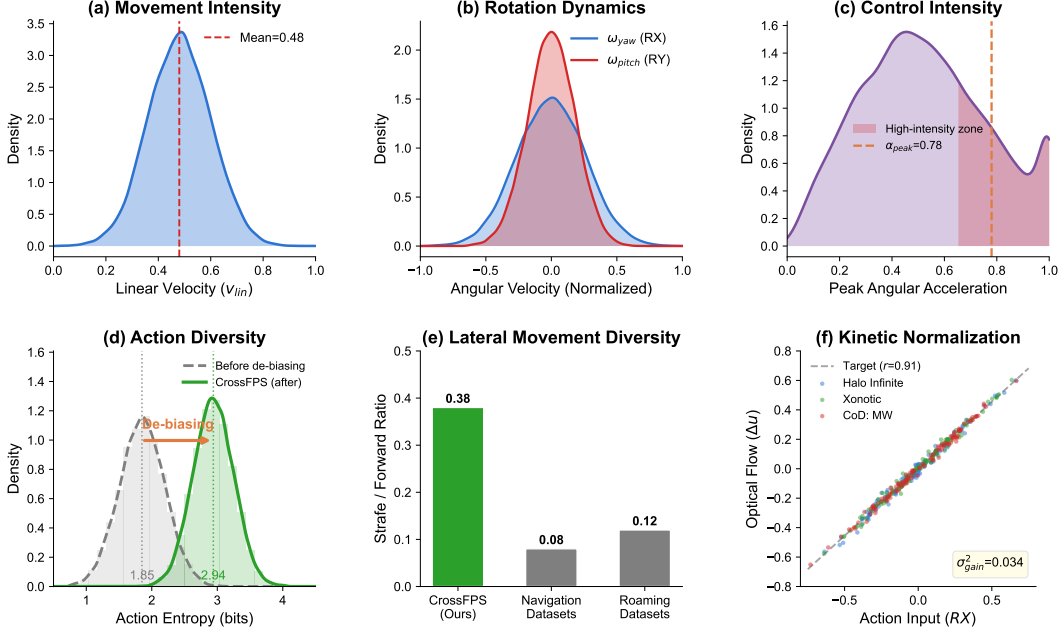


Figure 7: CrossFPS statistics. (a) Linear velocity distribution. (b) Angular velocity for yaw and pitch. (c) Peak angular acceleration with high-intensity zone. (d) Action entropy before and after de-biasing. (e) Strafe-to-forward ratio compared with navigation and roaming datasets. (f) Post-normalization kinetic consistency across three titles ($\sigma_{\text{gain}}^2 = 0.034$).

This ensures that SCOPE learns authentic *physical action-visual mappings* rather than memorizing game strategies. To achieve this, we process the raw gameplay recordings through a rigorous pipeline designed to enforce diversity, balance, and cross-game consistency, structured into four primary phases:

Spatial-Temporal Formatting. We first extract the active game area by cropping out streaming overlays and UI borders. Videos are split at scene transitions (e.g., death or loading screens) using frame-level visual similarity to ensure continuous gameplay. We then segment the recordings into non-overlapping 5-second windows and normalize the frame rate to a uniform 20 fps via temporal subsampling (for 60 fps sources) or interpolation (for 30 fps sources). Finally, game-specific UI elements (like chat boxes) are cropped out, and all clips are resized to 480×832 to maintain a 16:9 aspect ratio.

Quality Filtering and Action Balancing. Human gameplay inherently suffers from a long-tail distribution, heavily skewed toward low-intensity states (e.g., straight-line running). We first apply an activity filter (left-stick active $\geq 70\%$) to remove idle clips. To ensure adequate coverage of high-intensity dynamics, we compute the action entropy $H_i = -\sum_k p_k \log p_k$ and peak camera velocity for each clip. High-intensity clips (the top 15%, featuring rapid 180-degree flicks or jump chains) are oversampled by $3\times$. This step prevents the model from collapsing into generating only smooth, low-motion sequences.

Visual-Action De-biasing. To force the model to learn raw physics rather than strategic priors, we explicitly retain "inefficient" or counter-intuitive actions (e.g., firing at an empty sky, sprinting into walls). We identify these clips by computing the mutual information between the visual features from a pre-trained scene classifier and the discrete action sequences. Clips with the lowest mutual information (the bottom 20%) are flagged as "de-biased" samples and forcefully included in the training set. This teaches SCOPE that actions reliably trigger corresponding visual changes regardless of their strategic utility.

Cross-Game Kinetic Normalization. Different game engines map analog stick displacements to vastly different camera rotation speeds (e.g., identical stick displacement produces a 10° rotation in *Halo* but 30° in *Call of Duty*). To resolve the resulting gradient conflicts during multi-game joint training, we apply optical flow-based gain calibration. For each clip, we extract the mean pixel displacement $(\Delta u, \Delta v)$ caused by camera rotation and fit a linear gain model $(\Delta u \approx g_x \cdot RX)$. Camera signals are rescaled by $RX_{\text{norm}} = RX \cdot (\bar{g}_x / g_x)$, where \bar{g}_x is the dataset-wide mean gain. For static or highly occluded scenes where optical flow fails, we apply a 95th-percentile fallback normalization. Additionally, inverted axes (e.g., in *Xonotic*) are negated to establish a unified directional convention.

Prior to training, all 65,557 training clips passed a comprehensive integrity check (validating video readability, first-frame decodability, frame count, resolution, and action file completeness) with a 100% pass rate.

A.4 Text Caption Generation

To provide text conditioning during training, we generate scene descriptions for the first frame of every clip using Gemini [50]. Each caption follows a standardized two-sentence format:

- **Sentence 1** describes the environment: setting, lighting, architecture, and atmosphere.
- **Sentence 2** describes the player state and salient visual elements: weapon type, HUD indicators, nearby objects, and game-specific UI.

This structured format ensures consistent conditioning signals across all games while preserving scene-specific details. Representative examples from each game are shown in Figure 8–10, where the first frame used for caption generation and as the image-to-video condition is highlighted with a **green box**, and the corresponding frame-aligned action inputs are displayed below the frame sequence.

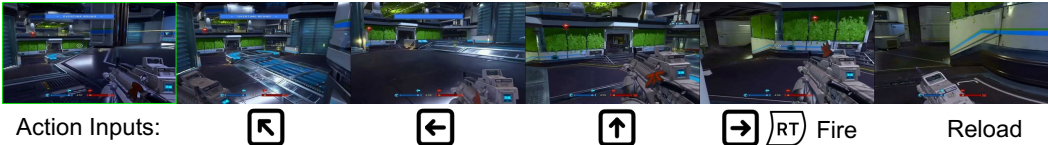


Figure 8: **Halo Infinite example.** The first frame (highlighted with a **green box**) is used for caption generation and as the image-to-video condition. The action input sequence shows forward movement with a rightward camera sweep followed by ADS activation. Caption: “A futuristic sci-fi indoor arena with multi-level platforms, neon blue lighting, green vegetation behind glass walls, and metallic surfaces during an overtime round. The player is holding a large rifle in a ready stance, with the score tied 0-0 at 4:57 remaining, and a crosshair centered on the screen.”

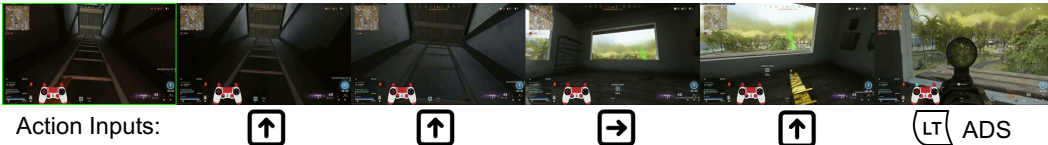


Figure 9: **Call of Duty: Warzone example.** The first frame (highlighted with a **green box**) is used for caption generation and as the image-to-video condition. The action input sequence shows a leftward camera rotation transitioning to forward movement with simultaneous fire and reload events. Caption: “A dark narrow stairwell inside a building in Caldera Capital City, with a wooden ladder leading upward through a dimly lit vertical shaft. The player is climbing the ladder while holding a weapon with 48 rounds, a minimap and kill feed visible on the HUD, and a controller overlay displayed at the bottom center of the screen.”

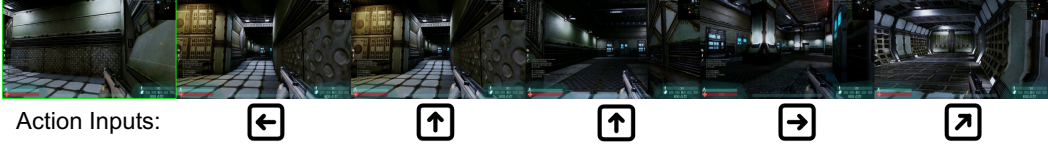


Figure 10: **Xonotic example.** The first frame (highlighted with a green box) is used for caption generation and as the image-to-video condition. The action input sequence shows leftward movement combined with forward camera motion, rightward sweep, and a diagonal turn. Caption: “A dark military-industrial interior room labeled ‘Computer Room’ with large metal panel walls featuring riveted circular patterns, grid-patterned flooring, and dim greenish lighting. The player is holding a tan assault rifle at hip level, with full health at 100, 30 rounds in the magazine, 800 points displayed, and running at 125 fps.”

B Implementation Details

The backbone model is Wan2.2-TI2V-5B [55] with 30 transformer layers, hidden dimension 3072, 24 attention heads, patch size [1, 2, 2], and FFN dimension 14336. The text encoder is UMT5-XXL producing 4096-dimensional embeddings. The VAE uses $8\times$ spatial compression and $4\times$ temporal compression. Each SCOPE module contains: a fusion MLP for continuous control processing, a cross-attention block for discrete event processing, and temporal RoPE embeddings. All output projections are zero-initialized so that modules produce no perturbation at initialization. The entire model (backbone + SCOPE modules) is trained end-to-end using AdamW with learning rate 10^{-5} , bfloat16 precision, gradient checkpointing, and batch size 1 per GPU across 8 NVIDIA GPUs for 500 epochs. We use the Accelerate library for distributed training with DDP.

B.1 Training and Inference Pseudocode

The complete training and inference procedures are given in Algorithm 1 and Algorithm 2.

Algorithm 1 SCOPE training

Require: p_{drop} : action dropout probability; \mathbf{a}_{null} : learnable null embedding

- 1: **repeat**
- 2: $(\mathbf{V}, \mathbf{a}_c, \mathbf{a}_d, \mathbf{c}_{\text{text}}) \sim \mathcal{D}$ {Sample from CrossFPS}
- 3: $\mathbf{z}_0 \leftarrow \text{VAE}_{\text{enc}}(\mathbf{V})$; condition on first-frame latent $\mathbf{z}_0^{(1)}$
- 4: $(\mathbf{a}_c, \mathbf{a}_d) \leftarrow \mathbf{a}_{\text{null}}$ with probability p_{drop} {Action dropout for CFG}
- 5: $t \sim \mathcal{U}(0, 1)$; $\epsilon \sim \mathcal{N}(\mathbf{0}, \mathbf{I})$; $\mathbf{z}_t \leftarrow (1 - t)\mathbf{z}_0 + t\epsilon$
- 6: $\mathbf{x} \leftarrow \text{Patchify}(\mathbf{z}_t)$
- 7: **for** $l = 1, \dots, L$ **do**
- 8: $\mathbf{x} \leftarrow \text{DiTBlock}_l(\mathbf{x}, \mathbf{c}_{\text{text}}, t)$ {Standard DiT: self-attn + text cross-attn}
- 9: $\hat{\mathbf{x}} \leftarrow \text{Reshape}(\mathbf{x})$ to per-pixel temporal sequences {Spatial selectivity}
- 10: $\Delta \mathbf{x}_c \leftarrow \text{SelfAttn}(\text{MLP}_{\text{fuse}}([\hat{\mathbf{x}}; \mathbf{a}_c]))$ {Continuous pathway}
- 11: $\Delta \mathbf{x}_d \leftarrow \text{CrossAttn}(Q=\hat{\mathbf{x}}, K=V=\text{MLP}_{\text{embed}}(\mathbf{a}_d))$ {Discrete pathway}
- 12: $\mathbf{x} \leftarrow \text{Reshape}(\hat{\mathbf{x}} + \Delta \mathbf{x}_c + \Delta \mathbf{x}_d)$; $\mathbf{x} \leftarrow \text{FFN}_l(\mathbf{x})$
- 13: **end for**
- 14: Take gradient step on $w(t) \|\mathbf{v}_\theta - (\epsilon - \mathbf{z}_0)\|^2$
- 15: **until** converged

C Evaluation Metrics

We evaluate the generated videos along three primary axes using eight metrics. All metrics are computed on the CrossFPS test set (1,378 clips) at a 480×832 resolution. A comprehensive summary of the evaluation metrics is provided in Table 8.

Algorithm 2 SCOPE inference with Action-CFG

Require: λ : guidance strength; \mathbf{I}_1 : first frame; $(\mathbf{a}_c, \mathbf{a}_d)$: action sequence; $t_1 > \dots > t_S$: schedule

- 1: $\mathbf{z}_0^{(1)} \leftarrow \text{VAE}_{\text{enc}}(\mathbf{I}_1)$; $\mathbf{z}_{t_1} \sim \mathcal{N}(\mathbf{0}, \mathbf{I})$
 - 2: **for** $s = 1, \dots, S$ **do**
 - 3: $\mathbf{v}_{\text{cond}} \leftarrow \mathbf{v}_\theta(\mathbf{z}_{t_s}, t_s, \mathbf{c}, \mathbf{a}_c, \mathbf{a}_d)$ {Conditional forward pass}
 - 4: $\mathbf{v}_{\text{uncond}} \leftarrow \mathbf{v}_\theta(\mathbf{z}_{t_s}, t_s, \mathbf{c}, \mathbf{a}_{\text{null}})$ {Unconditional forward pass}
 - 5: $\hat{\mathbf{v}} \leftarrow \mathbf{v}_{\text{uncond}} + \lambda(\mathbf{v}_{\text{cond}} - \mathbf{v}_{\text{uncond}})$ {Action-CFG}
 - 6: $\mathbf{z}_{t_{s+1}} \leftarrow \text{ODEStep}(\mathbf{z}_{t_s}, \hat{\mathbf{v}}, t_s \rightarrow t_{s+1})$
 - 7: **end for**
 - 8: **return** $\text{VAE}_{\text{dec}}(\mathbf{z}_{t_{S+1}})$
-

Table 8: Summary of Evaluation Metrics for Reactive Game World Models.

Evaluation Axis	Metric	Reference	Primary Focus
Action Responsiveness	Dynamic Degree	[23]	Quantifies overall video activity and motion magnitude. Measures average optical flow displacement between frames.
	Flow Score	[32]	
Spatial Stability	Photometric Smoothness	[17]	Evaluates pixel-level color consistency via backward-warping. Assesses 3D geometric consistency using depth reprojection.
	Depth Accuracy	[43]	
Visual Quality	JEPA Similarity	[6, 33]	Captures high-level semantic and physical structural fidelity. Measures the realism of the generated spatiotemporal distribution.
	FVD	[53]	
	LPIPS	[67]	Evaluates per-frame perceptual distortion and image clarity. Analyzes flow acceleration to penalize abrupt motion jitter.
	Motion Smoothness	[17, 66]	

C.1 Action Responsiveness

This axis measures whether generated videos exhibit genuine dynamic changes in response to sequential action inputs, heavily penalizing models that produce static or unresponsive outputs.

Dynamic Degree [23]. We extract spatiotemporal features from the generated video sequence to quantify the magnitude of inter-frame dynamic variation. By analyzing the intensity of object motion and global scene changes across frames, this metric produces a holistic score reflecting the overall activity level.

Flow Score [32]. We compute the average optical flow magnitude between consecutive frames. Let $F_t(x, y) \in \mathbb{R}^2$ denote the estimated optical flow vector at spatial coordinate (x, y) from frame I_t to I_{t+1} . The Flow Score across T frames with spatial dimensions $H \times W$ is defined as:

$$FS = \frac{1}{(T-1)HW} \sum_{t=1}^{T-1} \sum_{x=1}^W \sum_{y=1}^H \|F_t(x, y)\|_2$$

Higher scores indicate a larger motion amplitude; conversely, near-zero scores typically signal generation failure (i.e., frozen frames).

C.2 Spatial Stability

This axis measures whether generated videos maintain a consistent 3D geometric structure over time, directly penalizing spatial collapse, warping, or unauthorized object deformation.

Photometric Smoothness [17]. We evaluate pixel-level color consistency between adjacent frames. Using estimated depth maps and optical flow, we backward-warp pixels from the next frame I_{t+1} to the current frame I_t 's viewpoint to obtain the reconstructed frame \tilde{I}_t . The photometric error is measured as the average L_1 distance:

$$PS = \frac{1}{(T-1)HW} \sum_{t=1}^{T-1} \sum_{x=1}^W \sum_{y=1}^H \|I_t(x, y) - \tilde{I}_t(x, y)\|_1$$

Lower errors indicate highly stable photometric behavior devoid of flickering or texture artifacts.

Depth Accuracy [43]. We predict depth maps D_t for all generated frames using a pre-trained monocular depth estimator. Given the camera pose transformation $T_{t \rightarrow t+1}$, we reproject the 3D point cloud from the previous frame into the current frame to compute the reprojected depth \tilde{D}_{t+1} . We calculate the scale-invariant relative error between \tilde{D}_{t+1} and the directly estimated D_{t+1} . Higher accuracy confirms that the model rigidly maintains correct 3D scene geometry.

C.3 Visual Quality

This axis rigorously evaluates image clarity, perceptual realism, semantic fidelity, and motion coherence.

JEPA Similarity [6, 33]. We extract feature vectors from both generated videos V and ground-truth reference videos \hat{V} using a pre-trained Joint Embedding Predictive Architecture (V-JEPA). Because V-JEPA captures high-level semantic content without relying on strict pixel-level reconstruction, we compute the cosine similarity in its feature space ϕ :

$$S_{\text{JEPA}} = \frac{\phi(V) \cdot \phi(\hat{V})}{\|\phi(V)\|_2 \|\phi(\hat{V})\|_2}$$

Higher similarity demonstrates that the generated content preserves the semantic and physical structure of the reference sequence.

FVD [53]. We extract spatiotemporal features from both generated and real video collections using a pre-trained I3D network. Modeling the feature distributions of the real data and generated data as multivariate Gaussians $\mathcal{N}(\mu_r, \Sigma_r)$ and $\mathcal{N}(\mu_g, \Sigma_g)$, the Fréchet Video Distance is calculated as:

$$FVD = \|\mu_r - \mu_g\|_2^2 + \text{Tr}(\Sigma_r + \Sigma_g - 2(\Sigma_r \Sigma_g)^{1/2})$$

A lower FVD indicates that the generated spatiotemporal distribution more closely matches the real data distribution.

LPIPS [67]. We measure per-frame perceptual distortion by passing generated frames \hat{x} and reference frames x through a pre-trained VGG network. We compute the weighted L_2 distance between the normalized intermediate feature maps \hat{y}^l and y^l at each layer l :

$$LPIPS(x, \hat{x}) = \sum_l \frac{1}{H_l W_l} \sum_{i,j} \|w_l \odot (\hat{y}_{i,j}^l - y_{i,j}^l)\|_2^2$$

LPIPS correlates much more closely with human perception of blur and structural artifacts than traditional pixel-level metrics such as PSNR or SSIM.

Motion Smoothness [17, 66]. We analyze the temporal variation of optical flow fields by isolating the acceleration (the second-order derivative) of flow vectors across consecutive frame triplets. Let $A_t = F_{t+1} - F_t$ represent the change in optical flow. We penalize large magnitudes of A_t , as abrupt changes in motion trajectory or velocity manifest as visual jitter or stuttering. High motion smoothness scores indicate physically plausible, continuous inertial motion.

D Scalability Details

This section provides full numerical results for the scalability analysis discussed in Section 4.3, covering both training strategy comparisons and data scale/diversity ablations.

Training strategy details. Table 2 (main paper) reports three training regimes applied to the full 65K dataset: (1) *Frozen backbone*—only the 30 SCOPE modules are trained while all pretrained parameters are fixed; (2) *Two-stage*—SCOPE modules are first trained with a frozen backbone, then the entire model is fine-tuned jointly; (3) *End-to-end*—all parameters are trained from the start. The Frozen variant’s JEPA of 0.724 and Photometric Smoothness of 0.264 demonstrate that the SCOPE module functions effectively as a plug-and-play adapter. The Two-stage variant (JEPA 0.761) shows that partial backbone adaptation captures mid-level action-visual correlations.

Full end-to-end training (JEPA 0.806) yields the strongest results by enabling deep co-adaptation between the SCOPE modules and the backbone’s internal representations, particularly for Flow Score (15.57→17.13→18.24). Notably, even the Frozen variant’s Photometric Smoothness (0.264) remains far superior to the “w/o Spatial Selectivity” ablation (0.745), confirming that the per-pixel conditioning design itself—independent of backbone adaptation—drives out-of-scope stability.

Data scale and diversity configurations. We study how data volume and source diversity jointly influence model quality by constructing training subsets at five scales with controlled diversity levels. Starting from Halo series data (the largest single source in CrossFPS), we progressively include additional game families:

- **1K** — 1,000 clips randomly sampled from Halo Infinite (1 title).
- **5K** — 5,000 clips from Halo Infinite + Halo MCC (2 titles, same series).
- **10K** — 10,000 clips from Halo series + Call of Duty: Modern Warfare (3 titles, 2 series).
- **30K** — 30,000 clips from Halo series + CoD series + Xonotic (6 titles, 3 series).
- **65K (full)** — All 65,557 training clips across 7 titles (3 series).

At each scale, clips are randomly sampled from all available titles with balanced per-game ratios (capped at available clips per title). All configurations use single-stage training at 480×832 .

Table 9: Data scale and diversity ablation. Scale: number of training clips; Titles: number of distinct games; Series: number of distinct game franchises. All trained at 480×832 with single-stage strategy.

Scale	Titles	Series	Source Composition	FVD↓	LPIPS↓	Flow↑
1K	1	1	Halo Infinite	478.20	0.545	17.64
5K	2	1	Halo Infinite + Halo MCC	603.91	0.592	16.67
10K	3	2	Halo $\times 2$ + CoD:MW	1017.82	0.745	11.69
30K	6	3	Halo $\times 2$ + CoD $\times 3$ + Xonotic	799.70	0.666	16.84
65K	7	3	Full CrossFPS	690.30	0.601	18.24

Training strategy comparison at each scale. We additionally compare single-stage training (directly at 480×832) with progressive training ($248 \times 448 \rightarrow 480 \times 832$) at each data scale.

Table 10: **Training strategy comparison across data scales.** Progressive: low-resolution warm-up followed by high-resolution fine-tuning; Single-stage: trained directly at full resolution.

Scale	Strategy	FVD↓	LPIPS↓	Flow↑
1K (Halo only)	Progressive	612.35	0.621	15.82
1K (Halo only)	Single-stage	485.42	0.554	17.95
5K (Halo series)	Progressive	705.18	0.645	15.30
5K (Halo series)	Single-stage	621.76	0.589	16.54
10K (2 series)	Progressive	845.21	0.682	14.85
10K (2 series)	Single-stage	1032.55	0.741	11.23
30K (3 series)	Progressive	781.45	0.659	16.50
30K (3 series)	Single-stage	798.30	0.645	16.62
65K (full)	Progressive	756.28	0.652	17.12
65K (full)	Single-stage	690.30	0.601	18.24

Key observations. (1) At small scale with limited diversity (1K–5K, single series), single-stage training works well as the domain is homogeneous. (2) At intermediate scale with moderate diversity (10K, 2 series), cross-domain interference destabilizes single-stage training (FVD 1033 vs. 845 for progressive), as visually distinct game assets create conflicting gradients. (3) At full scale with maximum diversity (65K, 7 titles), sufficient multi-source variety provides natural regularization, and single-stage training surpasses progressive across all metrics. These results motivate our final design: single-stage training on the full multi-game dataset.